

Identification of Novel Functional Inhibitors of Acid Sphingomyelinase

Johannes Kornhuber^{1*}, Markus Muehlbacher^{1,2*}, Stefan Trapp³, Stefanie Pechmann¹, Astrid Friedl¹, Martin Reichel¹, Christiane Mühle¹, Lothar Terfloth⁴, Teja W. Groemer¹, Gudrun M. Spitzer², Klaus R. Liedl², Erich Gulbins⁵, Philipp Tripal¹

1 Department of Psychiatry and Psychotherapy, University of Erlangen, Erlangen, Germany, **2** Theoretical Chemistry, Center for Molecular Biosciences, University of Innsbruck, Innsbruck, Austria, **3** Department of Environmental Engineering, Technical University of Denmark, Lyngby, Denmark, **4** Molecular Networks GmbH, Erlangen, Germany, **5** Department of Molecular Biology, University of Duisburg-Essen, Essen, Germany

Abstract

We describe a hitherto unknown feature for 27 small drug-like molecules, namely functional inhibition of acid sphingomyelinase (ASM). These entities named FIASMAs (Functional Inhibitors of Acid SphingoMyelinAse), therefore, can be potentially used to treat diseases associated with enhanced activity of ASM, such as Alzheimer's disease, major depression, radiation- and chemotherapy-induced apoptosis and endotoxic shock syndrome. Residual activity of ASM measured in the presence of 10 μ M drug concentration shows a bimodal distribution; thus the tested drugs can be classified into two groups with lower and higher inhibitory activity. All FIASMAs share distinct physicochemical properties in showing lipophilic and weakly basic properties. Hierarchical clustering of Tanimoto coefficients revealed that FIASMAs occur among drugs of various chemical scaffolds. Moreover, FIASMAs more frequently violate Lipinski's Rule-of-Five than compounds without effect on ASM. Inhibition of ASM appears to be associated with good permeability across the blood-brain barrier. In the present investigation, we developed a novel structure-property-activity relationship by using a random forest-based binary classification learner. Virtual screening revealed that only six out of 768 (0.78%) compounds of natural products functionally inhibit ASM, whereas this inhibitory activity occurs in 135 out of 2028 (6.66%) drugs licensed for medical use in humans.

Citation: Kornhuber J, Muehlbacher M, Trapp S, Pechmann S, Friedl A, et al. (2011) Identification of Novel Functional Inhibitors of Acid Sphingomyelinase. PLoS ONE 6(8): e23852. doi:10.1371/journal.pone.0023852

Editor: Howard Riezman, University of Geneva, Switzerland

Received: June 4, 2011; **Accepted:** July 26, 2011; **Published:** August 31, 2011

Copyright: © 2011 Kornhuber et al. This is an open-access article distributed under the terms of the Creative Commons Attribution License, which permits unrestricted use, distribution, and reproduction in any medium, provided the original author and source are credited.

Funding: The work was supported in part by a grant from the DFG (KO 947/11-1, GU 335/23-1). The funders had no role in study design, data collection and analysis, decision to publish, or preparation of the manuscript. No additional external funding received for this study.

Competing Interests: LT is employed by a commercial company (Molecular Networks GmbH, Erlangen, Germany). The authors' employment does not alter their adherence to all the PLoS ONE policies on sharing data and materials, as detailed online in the guide for authors.

* E-mail: Johannes.Kornhuber@uk-erlangen.de

These authors contributed equally to this work.

Introduction

Acid sphingomyelinase (ASM, EC 3.1.4.12) is a lysosomal glycoprotein that catalyses the hydrolysis of sphingomyelin into ceramide and phosphorylcholine. Fusion of secretory lysosomes with the cell surface and translocation of lysosomal ASM onto the outer leaflet of the cell membrane plays an important role during stress response [1]. CD95 ligands and cytokines such as tumor necrosis factor- α , interleukin-1 and interferon- γ but also other stimuli including oxidative stress, reactive oxygen and nitrogen species, ionizing radiation, UV-C radiation, heat shock and other agents of stress, injury or infections by HIV or bacteria have been shown to stimulate ceramide production [2–7], assumed to be in part due to increased ASM activity. Ceramide, in turn, leads to membrane reorganization and downstream signalling that results in cell activation, very often cell stress or apoptosis. In addition to ASM, at least three other sphingomyelinases have been described in mammalian cells that vary in their pH optimum and cofactor dependency. Although these enzymes and an existing *de novo* synthesis pathway are alternative mechanisms for ceramide generation, activation of ASM itself has been proven to be critical for some cellular responses, such as apoptosis induced by reactive

oxygen and nitrogen species [3], chemotherapy drugs such as cisplatin [8], bacteria [5], radiation [9] and CD95 [10]. Furthermore, in contrast to other sphingomyelinases, ASM activity is tightly regulated [11].

Ceramide is further metabolized to sphingosine and sphingosine-1-phosphate by acid ceramidase (AC, EC 3.5.1.23) and sphingosine kinases. While the biological function of sphingosine is largely unknown, sphingosine-1-phosphate has been shown to be involved in cellular differentiation, proliferation and cell migration [12–16]. This dynamic balance between ceramide and sphingosine-1-phosphate is referred to as the “ceramide/sphingosine-1-phosphate rheostat” [17–19], maintaining the balance between growth and cell death.

ASM is best known for its involvement in Niemann-Pick disease, a lysosomal storage disease due to an inherited enzyme deficiency [20]. Pathological reduction of ASM activity may be caused by mutations in the ASM gene itself. The severity of Niemann-Pick disease correlates with the decrease of ASM activity [21]. However, studies using cells derived from Niemann-Pick disease patients or from ASM knock-out mice revealed that the deficiency of this enzyme might also have beneficial consequences, including anti-apoptotic and cytoprotective effects. In fact, there is increasing

evidence that ASM activation and ceramide accumulation play a central role in the development of common human diseases (reviewed in Smith & Schuchman [22]). Reports have been published of aberrant activation of ASM and/or altered levels of ceramide, for instance, for several psychiatric and neurological disorders such as major depression [23–25], morphine antinociceptive tolerance [26], Alzheimer's disease [27–29], spinal cord injury [30] and seizure disorder [31].

Therefore, ASM inhibitors hold promise for a number of new clinical therapies and might be used to prevent apoptosis and other negative effects occurring in different disease states such as in ischemia, stroke, Alzheimer's dementia, Parkinson's disease, Huntington's chorea, and of certain infections, in endotoxemia, and in atherosclerosis, and for the therapy of major depressive disorder [23,32–39]. Currently, only few examples of inhibitors directly interacting with ASM are known. These substances include physiological inhibitors of ASM such as phosphatidyl-*myo*-inositol-3,4,5-trisphosphate [40], L- α -phosphatidyl-D-*myo*-inositol-3,5-bisphosphate [41] and non-natural direct inhibitors of ASM, such as SMA-7 [42] and AD2765 [43]. A high throughput screening for direct ASM inhibitors was unsuccessful in finding lead structures [44]. The rational development of compounds that block ASM by direct interaction with the enzyme is difficult, since the crystal structure of the enzyme is not yet available. On the other hand, it has been known since the 1970s that some weak organic bases have the potential to reduce the activity of ASM [23,45–47]. It has been suggested that ASM is bound to intralysosomal membranes, and thereby protected against its own proteolytic inactivation. Weak bases, such as desipramine **168** (for numbering of compounds see Table S1), strongly accumulate in acidic intracellular compartments like lysosomes [48,49], a phenomenon called 'acid trapping' and in the case of lysosomes 'lysosomotropism'. This accumulation of desipramine **168** results in detachment of the ASM from the inner lysosomal membrane [50] and its subsequent inactivation, probably by proteolytic degradation [51]. Weak bases, therefore, do not directly inhibit ASM, but result in a *functional* inhibition of ASM. We have thus proposed the acronym FIASMA for Functional Inhibitor of Acid SphingoMyelinAse [39]. According to this model, functional inhibition of ASM requires high lysosomal concentrations of a weak basic drug.

Previously, we have shown that functional inhibition of ASM is related to high pKa- and high logP-values and have characterized several new FIASMAs, including the antidepressant drugs doxepine **63**, fluoxetine **104**, maprotilin **109**, nortriptyline **114**, paroxetine **118** and sertraline **124** [52]. The aims of the present study were (1) to identify more FIASMAs, (2) to further improve the *in silico* prediction of functional ASM inhibition by developing compact and easily-interpretable models with high internal consistency, (3) to investigate the relationship between permeation of the blood-brain barrier and functional inhibition of ASM and (4) to study the distribution of FIASMAs across different classes of drugs licensed for medical use in humans.

Using the present knowledge about lysosomal accumulation and drug-membrane interaction as prerequisite to functional inhibition of ASM, we developed the following hypotheses: FIASMAs (1) have shared structural and physicochemical properties allowing high lysosomal drug concentrations, compatible with partitioning into the inner surface of the lysosomal membrane and alteration of electrostatic membrane properties. We hypothesize that FIASMAs (2) will be found in different *therapeutic* drug classes and (3) belong to diverse *structural* drug classes. To reach the lysosome, functional inhibition of ASM requires penetration of drugs through biological membranes, comparable to substances crossing the blood-brain

barrier (BBB). We therefore hypothesize (4) that FIASMAs also penetrate the BBB and (5) are therefore overrepresented in drugs active in the central nervous system (CNS).

Results and Discussion

Identification of novel FIASMAs

We have previously reported functional inhibition of ASM in cell culture for a wide range of compounds at a concentration of 10 μ M for 30 min incubation time [52], based on initial experiments with fluoxetine **104**. Using a cell-based simulation model, we have meanwhile realized that very high logP- or pKa-values or the presence of two basic nitrogen atoms leads to slow accumulation kinetics [49]. Therefore, we have also tested longer incubation times for such compounds (Table S1) and found lower residual activities of ASM than previously reported for alverine **40**, astemizole **43**, bepridile **46**, camylofine **50**, cloperastine **56**, dicyclomine **98**, drofenine **64**, mebeverine **110**, mibefradile **74**, pimoziide **81** and thioridazine **32** (see Table S1). Several of these substances that were measured [52] as not functionally inhibiting ASM (residual activity of ASM above 50% of control value) are actually FIASMAs when prolonged incubation times are used (alverine **40**, dicyclomine **98**, mebeverine **110**, mibefradile **74**, pimoziide **81**). Our results demonstrate that it is important to consider slow lysosomal accumulation kinetics in compounds with very high pKa- and/or very high logP-values and in compounds with two basic nitrogen atoms. In addition to identifying five more of the previously-tested 101 compounds [52] as FIASMAs taking their slower lysosomal accumulation into account (see Table S1: alverine **40**, dicyclomine **98**, mebeverine **110**, mibefradile **74**, pimoziide **81**), we have identified 22 other previously unknown FIASMAs out of our new set of 175 small drug-like compounds (residual activity of ASM of $\leq 50\%$: aprindine **141**, biperidene **149**, carvedilol **160**, cepharrantine **161**, clemastine **170**, clofazimine **172**, conessine **175**, desloratadine **182**, dimebon **189**, emetine **196**, flupenthixol **208**, fluphenazine **209**, fluvoxamine **210**, hydroxyzin **219**, loperamide **227**, mebhydroline **229**, perphenazine **249**, profenamine **258**, sertindole **277**, solasodine **278**, tomatidine **291**, zolantidine **276**). Four of them (dimebon **189**: residual ASM activity 44.1%; fluvoxamine **192**: residual ASM activity 37.4%; hydroxyzin **219**: residual ASM activity 43.0%; mebhydroline **207**: residual ASM activity 41.9%) were classified as FIASMAs albeit with less reliability due to experimental error. To the best of our knowledge, functional inhibition of ASM has not previously been described for any of the compounds presented here. Looking at the whole group of FIASMAs which we experimentally investigated ($n = 72$, Kornhuber et al. 2008 [52] and Table 1), we noticed some general characteristics. These compounds had moderate to high logP-values (ACD10; mean \pm SD: 5.45 ± 1.13 ; range: 2.03–8.89) and possessed at least one basic nitrogen atom responsible for moderate to high pKa-values (ACD10; mean \pm SD: 9.04 ± 1.18 ; range: 4.81–11.20). This qualifies all FIASMAs as cationic amphiphilic drugs. Most FIASMAs had a molecular weight below 500 (ACD10; mean \pm SD: 366.3 ± 85.1 ; range: 263.4–645.3).

Functional inhibition of ASM is bimodally distributed

Analysis of the whole set of compounds ($n = 276$), reveals a bimodal distribution of drugs with respect to functional inhibition of ASM (Figure 1) and a significant deviation from the normal distribution (Kolmogoroff-Smirnov: $p < 0.001$), with the lowest occurrence of FIASMAs at a residual activity between 50 and 60%. Both subpeaks of the bimodal distribution did not significantly deviate from a normal distribution. The reason for

Table 1. Newly-identified FIASMAs.

Generic name or substance code	CID	ATC code	FDA status [70]
Alverine 40	3678	A03AX08	Not listed
Mibefradile 74	60663	C08CX01	Not listed
Pimozide 81	16362	N05AG02	Prescription drug
Dicyclomine 98	3042	A03AA07	Prescription drug
Mebeverine 110	4031	A03AA04	Not listed
Aprindine 141	2218	C01BB04	Not listed
Biperidene 149	2381	N04AA02	Prescription drug
Carvedilol 160	2585	C07AG02	Prescription drug
Cepharantine 161	360849	Not listed	Not listed
Clemastine 170	26987	D04AA14	Prescription drug
Clofazimine 172	2794	J04BA01	Prescription drug
Conessine 175	441082	Not listed	Not listed
Desloratadine 182	124087	R06AX27	Prescription drug
Dimebon 189	197033	Not listed	Not listed
Emetine 196	10219	P01AX02	Not listed
Flupenthixol 208	5281881	N05AF01	Not listed
Fluphenazine 209	3372	N05AB02	Prescription drug
Fluvoxamine 210	5324346	N06AB08	Prescription drug
Hydroxyzin 219	3658	N05BB01	Prescription drug
Loperamide 227	3955	A07DA03	Prescription drug
Mebhydroline 229	22530	R06AX15	Not listed
Perphenazine 249	4748	N05AB03	Prescription drug
Profenamine 258	3290	N04AA05	Discontinued drug
Sertindole 277	60149	N05AE03	Not listed
Solasodine 278	442985	Not listed	Not listed
Tomatidine 291	65576	Not listed	Not listed
Zolantidine 306	91769	Not listed	Not listed

See Table S1 for further details and numbering of compounds.

CID = PubChem Compound ID.

doi:10.1371/journal.pone.0023852.t001

the bimodal distribution may be the inevitable presence of physicochemical properties that are non-linearly related to lysosomal drug accumulation and that work in a synergistic way. Since our experimentally-tested compounds were not randomly chosen, a selection bias might also contribute to the bimodal distribution.

Random forest learners provide a good binary prediction of functional inhibition of ASM

We divided the dataset into two groups – active compounds ($\leq 50\%$ residual ASM activity, class 1, $n=72$) and inactive compounds ($>50\%$ residual ASM activity, class 0, $n=204$). Usually, dichotomizing continuous variables results in a number of statistical problems, including a loss of statistical power to detect a relation between a variable and outcome [53–55]. In our data, dichotomization is justified by the pronounced bimodal distribution. We performed a *qualitative prediction* of functional inhibition of ASM using the whole set and random forest learners. The prediction accuracy in the set increased with the number of attributes used. A high precision of prediction was reached with $n=4$ attributes, which is only marginally improved by adding a fifth descriptor (Table 2). The successful 4-descriptor combination

included $\log\text{PACD10_logWeight}$, $\text{pKa1_plus_pKa2ACD10mod}$, pKaMA_ACD10 and si_Weight_vsa_pol . These four descriptors were only moderately correlated to each other (Spearman rank correlation r^2 between -0.598 and 0.314 , $n=276$) and thus provide complementary information. The descriptors $\log\text{P}$ and pKa have been discussed most frequently in the context of lysosomal accumulation [48,49]. Intermediate to high $\log\text{P}$ values have previously been identified as an important precondition for lysosomal accumulation. However, $\log\text{PACD10_logWeight}$ ($=\log\text{PACD10}-\frac{1}{2}\log\text{MW}$) is more closely related to the diffusion of small molecules through lipid phases than $\log\text{P}$ itself and has been used to predict BBB permeation [56,57]. The descriptor $\text{pKa1_plus_pKa2ACD10mod}$ represents the sum of the pKa -values of the most basic and the second-most basic nitrogen atoms and thus takes into account the impact of a second basic functional group. The descriptor pKaMA_ACD10 represents the pKa -value of the most acidic group and thus guarantees that acids are correctly classified as being inactive. vsa_pol is an approximation to the sum of van-der-Waals surface areas of polar atoms and has been described to predict BBB permeability [58]. For this descriptor, both hydrogen bond donors and acceptors count as polar atoms. The size-intensive form of the descriptor was chosen here. The four molecular descriptors thus represent electrostatic ($\text{pKa1_plus_pKa2ACD10mod}$, pKaMA_ACD10), hydrophobic ($\log\text{PACD10_logWeight}$), polar (vsa_pol) and steric (weight) properties of the molecules. No further steric descriptors were chosen into the model. The reason for this is probably the low variance of steric descriptors as all of the compounds investigated here are small drug-like molecules. The 4-descriptor model presented here is simple, easy to interpret, has high internal consistency and is meaningful in the context of lysosomal accumulation (Table 2). None of the 276 compounds was incorrectly predicted by the 4-descriptor model.

Based on a smaller set of experimentally investigated compounds ($n=101$) and a decision tree learner we had previously suggested a 3-descriptor model ($\log\text{PACD10}$, pKa1ACD10 , k) for qualitative prediction of functional inhibition of ASM [52]. Applying this 3-descriptor model on the large experimental dataset available in the present study ($n=276$) still results in a reasonable good prediction of functional inhibition of ASM (mean bootstrap-validated Youden-index: 0.575 ± 0.085 , mean bootstrap-validated accuracy 0.831 ± 0.033 , Youden-index without bootstrap-validation 1.0, accuracy without bootstrap-validation 1.0). However, the descriptor-combinations presented here (Table 2) outperform the previous prediction system. The previously suggested model [52] was now improved in several ways by using advanced molecular descriptors (e.g. $\log\text{PACD10}-\frac{1}{2}\log\text{MW}$ instead of $\log\text{PACD10}$; $\text{pKa1ACD10}+\text{pKa2ACD10}$ instead of pKa1ACD10), by using four instead of three molecular descriptors, by using a random forest learner instead of a simple decision tree learner and by using rigorous model validation. This led to a much more precise prediction system.

Whenever a structure-property-activity relationship (SPAR) model is built, there is a probability that the best model is chance correlation. We therefore performed a response permutation test (also known as Y-scrambling [59–61]). If a strong correlation remains between the selected descriptors and the randomly permuted response, the significance of the proposed model is suspect. The 4-descriptor model ($\log\text{PACD10_logWeight}$, $\text{pKa1_plus_pKa2ACD10mod}$, pKaMA_ACD10 , si_Weight_vsa_pol) was recalculated for a randomly reordered response. This procedure was performed 1000 times using different random seeds for permutation, resulting in a mean bootstrapping validated Youden-index of 0.001 ± 0.034 and a mean bootstrapping

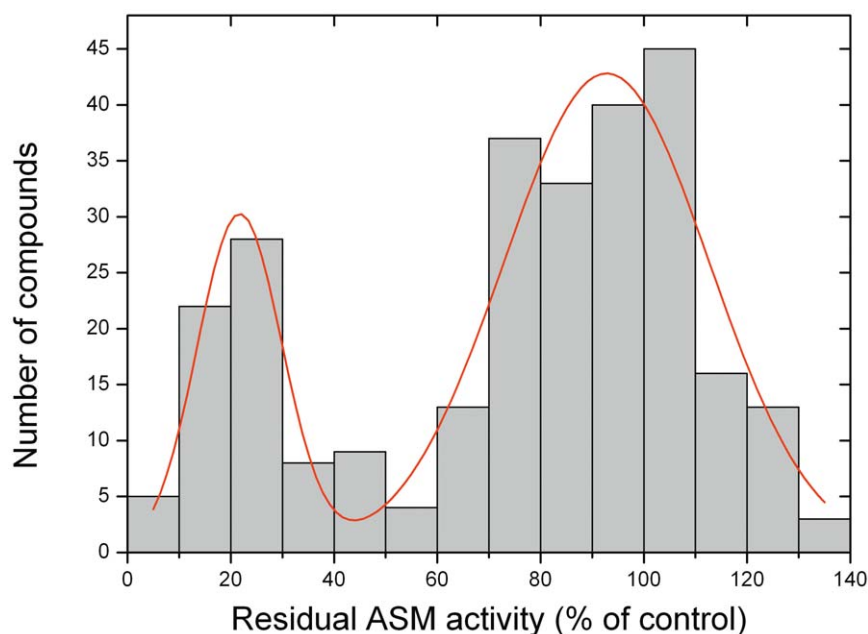


Figure 1. Analyzed compounds show a bimodal distribution with respect to functional inhibition of ASM. The histogram includes results of 276 experimentally investigated compounds (see Table S1). The line represents a Gaussian fit to the two peaks. doi:10.1371/journal.pone.0023852.g001

validated accuracy of 0.675 ± 0.014 for the whole experimental set ($n = 276$). The performance of the 4-descriptor model applied to the original dataset is therefore more than 15 standard deviations above random (mean accuracy in the whole experimental set = 0.884) indicating a large distance between a random response model and a true response model. The whole set comprised 276 compounds, 204 of them in class 0 (inactive) and 72 in class 1 (active). A model assuming all compounds would belong to class 0 (zero rule model) would have an accuracy of 0.739. The accuracy of the chosen model applied to the original dataset is significantly higher than the zero rule model, whereas the model applied to randomly reordered response values has a performance which is even lower than the zero rule model.

The whole process from data pre-processing to model generation and interpretation was in accordance with the OECD/IOMC guidelines for quantitative structure-activity rela-

tionship development [62]. This means that our study had (1) a defined endpoint, (2) an unambiguous algorithm, (3) a defined domain of applicability, (4) appropriate measures of goodness-of-fit, robustness and predictivity and (5) a mechanistic interpretation.

Additive effect of FIASMAs

Co-application of structurally diverse FIASMAs results in an additive functional inhibition of ASM, suggesting that these compounds share the same mechanism of inhibition. This is exemplified here by the additive effect of amitriptyline **6** and fluoxetine **104** (Figure 2).

FIASMAs tend to cross the blood-brain barrier

The blood-brain barrier (BBB) is a selective barrier formed by the endothelial cells that line cerebral microvessels [63]. Tight junctions between adjacent endothelial cells force most molecular

Table 2. Descriptor combinations were selected by a 200-fold bootstrap-validated Youden-index based on a binary random forest learner using the whole experimental set.

n	Descriptors	Mean 200fold bootstrap-validation		Final model without validation	
		Youden-index Mean \pm SD	Accuracy Mean \pm SD	Youden-index	Accuracy
1	logPACD10_logWeight	0.294 \pm 0.107	0.736 \pm 0.038	0.850	0.949
2	logPACD10_logWeight, pKa1_plus_pKa2ACD10mod	0.567 \pm 0.090	0.829 \pm 0.031	0.967	0.989
3	logPACD10_logWeight, pKa1_plus_pKa2ACD10mod, pKaMA_ACD10	0.626 \pm 0.087	0.852 \pm 0.031	0.990	0.993
4	logPACD10_logWeight, pKa1_plus_pKa2ACD10mod, pKaMA_ACD10, si_Weight_vsa_pol	0.680 \pm 0.087	0.884 \pm 0.030	1.000	1.000
5	logPACD10_logWeight, pKa1_plus_pKa2ACD10mod, pKaMA_ACD10, si_Weight_vsa_pol, si_Weight_prot_n_PI	0.714 \pm 0.086	0.897 \pm 0.027	1.000	1.000

A 4-descriptor combination provided high internal consistency, which is only marginally improved by addition of a fifth descriptor. Bootstrap-validated performance measures are given as mean \pm SD values.

doi:10.1371/journal.pone.0023852.t002

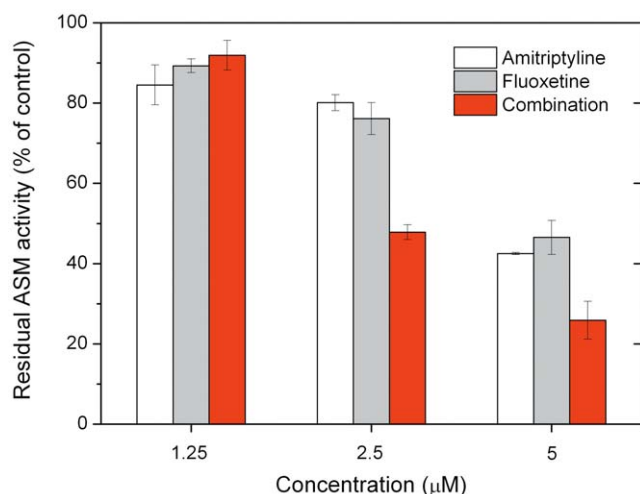


Figure 2. FIASMAs work in an additive way: The combination of a subthreshold-concentration of amitriptyline 6 and fluoxetine 104 (2.5 µM) results in functional inhibition of ASM. This effect is also evident at higher concentrations. Mean values \pm SD from 3 experiments are given.
doi:10.1371/journal.pone.0023852.g002

traffic across the BBB to take the transcellular route [64]. Small lipophilic agents can diffuse freely through the lipid membranes. Most CNS-active drugs use this transcellular lipophilic pathway. Compounds entering the brain have to cross two membrane barriers (both luminal and abluminal plasma membrane) and the cytoplasm of the endothelial cells in brain capillaries. FIASMAs have to go a similar way through the cell to reach the lysosome: they cross two membrane barriers (plasma membrane of the cell, lysosomal membrane) and the cytoplasm. Therefore an analogy between the BBB and the blood-lysosomal barrier can be assumed. For 64 of the 276 compounds investigated here, we found experimental \log_{BB} values (logarithmic ratio between the concentration of a compound in brain and blood) in the literature. When residual ASM activity is plotted against \log_{BB} values (Figure 3), it is apparent that functional inhibition of ASM (residual activity $\leq 50\%$) is found only for compounds that efficiently cross the BBB ($\log_{BB} \geq 0$).

FIASMAs violate Lipinski's Rule-of-Five more often than compounds without effect on ASM

We investigated whether or not our experimentally tested compounds ($n = 276$, Table S1) are in agreement with Lipinski's Rule-of-Five [65]. While 59 of 204 (28.9%) of compounds lacking a significant effect on ASM activity violated the Lipinski's Rule-of-Five, violation occurred in 37 of 72 (51.4%) of FIASMAs (chi-square test, $p = 0.001$, Table 3). In most of the FIASMAs violation of the Rule-of-Five was due to high lipophilicity. Nevertheless, FIASMAs are orally active and most of them are probably also CNS-active drugs.

Virtual screening shows that FIASMAs are enriched in groups of drugs acting at excitable cells but are rare among natural products

Most of the clinically approved compounds have been developed without specific goals regarding $\log P$ - and pK_a -values. Therefore, there should be no remarkable differences in these physicochemical properties between groups of drugs approved for medical use. To get a complete picture of the distribution of

functional inhibition of ASM within approved drugs, we used the Anatomical Therapeutic Chemical (ATC) drug classification system recommended by the World Health Organization (WHO). Based on the random forest model described above, we analyzed a total of 2440 compounds distributed across 86 third-level drug groups of the ATC codes (with several substances occurring more than once; 2028 different compounds) by a virtual screening approach and found physicochemical characteristics indicative of functional inhibition of ASM in 157 of the 2440 ATC-listed compounds (6.43%). Since some of the drugs in the ATC system are chemically identical, but have a unique ATC-code because of their different clinical indications, a total of 135 of 2028 unique compounds (6.66%) was predicted to functionally inhibit ASM. The distribution of the 157 functional ASM inhibitors across the 86 pharmacologically relevant therapeutic groups significantly deviated from the expected values (Fisher's exact test, $p < 0.001$), but clustered clearly in a few groups. The multiple test correction on Fisher p -values revealed a significant overrepresentation of FIASMAs in only a few therapeutic groups, namely A03 (drugs for functional gastrointestinal disorders), A15 (appetite stimulants), C08 (calcium channel blockers), D04 (antipruritics), N04 (anti-parkinson drugs), N05 (psycholeptics), N06 (psychoanaleptics) and R06 (antihistamines for systemic use). Since group size of the ATC second level drug groups varies strongly, the p -value has a limited explanatory power. From a biological point of view, groups with a high fraction of FIASMAs may be still of interest, even if the p -value is not significant owing to the small size of the group, such as A04 (antiemetics and antinauseants). One common feature of these ATC subgroups with a significant overrepresentation of FIASMAs is the pharmacodynamic involvement of excitable cells where many FIASMAs appear to act primarily. Furthermore, it is evident, that several of the second-level ATC subgroups with a significant number of FIASMAs belong to the CNS active groups (N04, N05, N06).

In contrast to approved drugs for medical use, we found by virtual screening that FIASMAs are rare in natural products. The molecular descriptors necessary for application of the model were calculable in 787 of the 800 "Pure Natural Products" [66]. Two compounds with quaternary nitrogen atoms were excluded. Then we removed 17 duplicates. In six of the remaining 768 compounds (0.78%) the model indicated functional inhibition of ASM. Five of these predicted compounds were also part of the experimental set (Table S1): cepharanthine **161**, conessine **175**, emetine **196**, solasodine **278** and tomatidine **291** and did indeed show functional inhibition of ASM. The rate of predicted FIASMAs in natural products is much lower than the rate of predicted FIASMAs observed in drugs licensed for medical use in humans (6.66%). The applicability domain of our prediction model is small drug-like molecules. The set of Pure Natural Products differs in chemical space from the small drug-like molecules, meaning that these results have to be interpreted with caution.

FIASMAs are structurally heterogeneous

Chemical space and structural diversity are important when comparing different sets of compounds. It is not valid to extend results obtained in one set of compounds to other compound collections without taking into account structural diversity. In order to compare the degree of structural diversity between sets of compounds, we have developed a new and simple measure termed "relative structural diversity" (div_{rel}). This simple measure uses a hierarchical clustering of Tanimoto-coefficients [67] based on 2D-fingerprints (see experimental section) and may be used in addition to more complicated indicators of structural diversity [68]. The div_{rel} of the FIASMAs ($n = 72$, $\text{div}_{rel} = 0.667$) is somewhat lower but

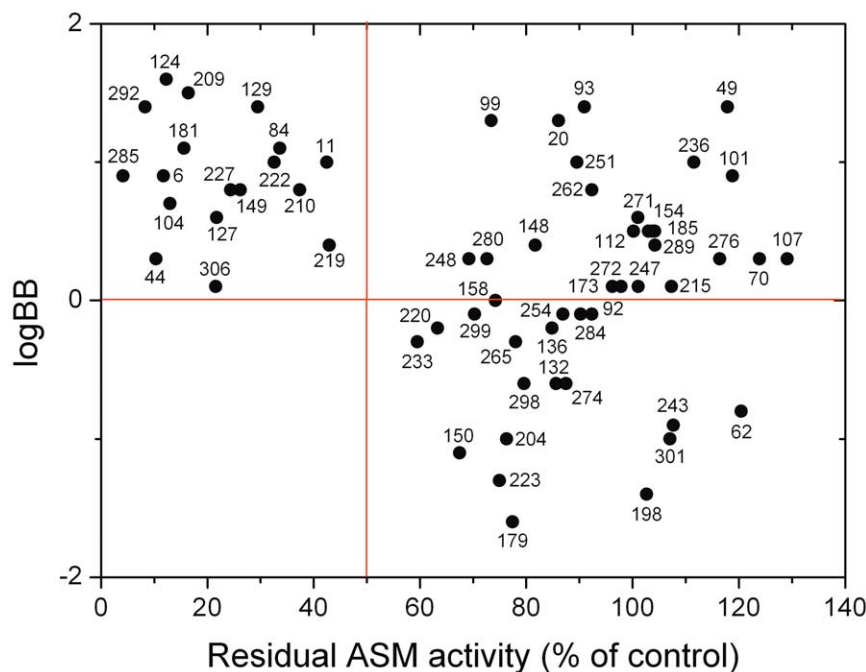


Figure 3. Functional inhibition of ASM appears to be associated with good passive diffusion across the blood-brain barrier. Experimental logBB values were compiled from the literature, with values greater than 0 indicating good blood-brain barrier permeability. Functional inhibition of ASM was experimentally determined in cell culture; residual ASM activity below 50% relative to control cells indicates active compounds. See also results in Table S1. doi:10.1371/journal.pone.0023852.g003

still high compared to the div_{rel} of the whole experimental set ($n = 276$, $div_{rel} = 0.711$). For comparison, div_{rel} is similar in the set of ATC compounds investigated ($n = 2028$, $div_{rel} = 0.709$) as well as in the set of natural products ($n = 768$, $div_{rel} = 0.747$) (Table 4). Thus, the molecular structure of FIASMAs varies widely, as indicated by the high number of clusters. This is supported by the fact that FIASMAs represent different therapeutic classes and different structural classes as evidenced by their ATC-codes (see Table 1). Our results prove that functional inhibition of ASM does not depend on a specific molecular drug class. Instead of specific structural prerequisites, functional inhibition of ASM requires specific physicochemical characteristics of compounds, resulting in high intra-lysosomal concentrations and partitioning of the drug into the inner leaf of the lysosomal membrane.

In the current study we used several different compound collections. The experimental set investigated here is showing comparable div_{rel} values to the ATC set. It is therefore appropriate to apply conclusions from the experimental set onto the larger ATC collection. The set of 72 FIASMAs is a subset of the

experimental set, which in turn is largely a subset of the ATC drug library. Therefore, these three sets occupy a comparable region of the chemical space, as all these sets are mainly composed of small drug like molecules. The Pure Natural Products cannot easily be compared to the drug-like molecules as their chemical space differs.

Clinical implications of the findings presented here

Most of the newly defined FIASMAs described here are included in the WHO drug list of approved and essential medicines [69] and about half of them appear in the US Food and Drug Administration (FDA)-approved drug list [70] (Table 1). These substances not only possess a low toxicity but also a record of a long-term clinical experience – some have been in use for the last five decades. FIASMAs have a number of favourable properties in the context of clinical application [39], suggesting the potential for rapid advancement into preclinical and/or clinical trials. The therapeutic consequences of functional

Table 3. FIASMAs frequently violate Lipinski's Rule-of-Five.

	Experimentally-determined ASM inhibitory activity	
	FIASMA	Not acting as FIASMA
Rule-of-Five = 0	35	145
Rule-of-Five > 0	37	59

Chi-square-test, $p = 0.001$.

Violation was assumed when there was a contradiction to any of the four rules. Violation of Lipinski's Rule-of-Five was calculated by ACD10 for all compounds with experimentally-determined ASM activity ($n = 276$).

doi:10.1371/journal.pone.0023852.t003

Table 4. Comparison of the relative structural diversity of the compound sets investigated here.

	n	div_{rel}
FIASMAs	72	0.667
Whole experimental set	276	0.711
ATC-set	2028	0.709
Pure Natural Products	768	0.747

Structural diversity was estimated by a new measure called relative structural diversity (div_{rel} , see experimental section). The set of FIASMAs is a subset of the whole experimental set investigated here.

doi:10.1371/journal.pone.0023852.t004

inhibition of ASM are yet poorly understood, however they may induce a number of clinically desired effects. Ceramide and its metabolite sphingosine-1-phosphate have been shown to antagonistically regulate apoptosis, cellular differentiation, proliferation and cell migration. Inhibition of ASM results in anti-apoptotic, proliferative and anti-inflammatory effects. Furthermore, ASM could play a key role in the pathophysiology of depression and in the action of antidepressant drugs [23]. Inhibitors of ASM therefore hold promise for a number of new clinical therapies. Several examples are given here: Induction of stroke by experimental ischemia of the brain was shown to correlate with an activation of the ASM and a release of ceramide [71,72]. Importantly, ASM-deficient mice were protected from tissue damage caused by focal cerebral ischemia. Furthermore, the ethanol-induced neuronal cell death is mediated, at least in part, by activation of ASM and generation of ceramide [73]. In addition, the lethal gastrointestinal syndrome, which limits the efficacy of radiation and chemotherapy, apparently results from apoptotic damage of the endothelial cells of the microvasculature of the small intestine. Genetic inactivation of ASM prevents this toxicity [74]. Infection induced by the human immunodeficiency virus type I (HIV-1) serves as a further example. HIV-1 induces a dramatic depletion of CD4+ T cells in infected individuals, finally leading to AIDS (acquired immunodeficiency syndrome). The massive loss of CD4 T-lymphocytes is assumed to result from apoptosis, probably due to enhanced sphingomyelin breakdown and accumulation of intracellular ceramide [75]. Interestingly, HIV-1 infected long-term nonprogressors have less elevated lymphocyte-associated ceramide than subjects with evolving AIDS [76], which is paralleled by a lower frequency of apoptotic CD4 and CD8 cells in long-term nonprogressors compared to patients with AIDS [77]. The endotoxic shock syndrome, which is characterized by systemic inflammation, multiple organ damage, circulatory collapse and death, is caused by disseminated endothelial apoptosis sequentially mediated by TNF and ceramide generation [78]. Blocking of this cascade by ASM inhibitors should be preventive and/or therapeutic against the endotoxic shock syndrome. Finally, an imbalance between ASM and acid ceramidase followed by ceramide accumulation has been demonstrated in the hereditary disease cystic fibrosis [79]. In experimental animals, FIASMAs normalize pulmonary ceramide and inflammation [80]. In a clinical pilot study, amitriptyline **6** led to an improved respiratory function in affected patients [81]. Further examples include the treatment of e.g. Alzheimer's disease, major depression, inflammatory bowel disease [42], liver cell death and anaemia occurring in Wilson disease, and pulmonary edema in acute lung injury [82]. Recently, it has been shown that gilenya (FTY720), a drug licensed for treatment of multiple sclerosis, acts as a FIASMA [83]. This novel mechanism of action may explain at least in part the beneficial effects of gilenya in multiple sclerosis.

AC is a lysosomal enzyme degrading ceramide to sphingosine. Cationic amphiphilic agents like desipramine, chlorpromazine and chloroquine have been shown to result in both, a reduced level of AC protein and in an increased level of cellular ceramide [84,85]. Despite its potential importance, the influence of medically used drugs on AC has not yet been systematically studied. In a cell culture-based pilot study on more than 100 small drug-like compounds (CM, unpublished), FIASMAs had a significantly stronger AC inhibitory effect than non-FIASMAs. However, the effect on AC was less pronounced compared to their effect on ASM as none of the compounds reduced AC activity to levels below 50%. Moreover, because of the considerably lower enzyme activity of the AC compared to ASM (about 25 fold in cell lysates using fluorescently labelled substrates; CM unpublished), the

absolute net effect of potentially inhibitory drugs is expected to be dominated by their influence on ASM. The observation of reduced ceramide levels in the mouse hippocampus after application of amitriptyline or fluoxetine (EG, unpublished results) is in agreement with this hypothesis. Nevertheless, the potential dual effect of small drug-like compounds on ASM as well as AC deserves further research with the aim to identify compounds with specific inhibitory activity for therapeutic use.

Strengths and limitations of the study

Strength: We identified 27 novel FIASMAs, many of them FDA-approved for clinical use in humans. Model construction was based on a large number of experimentally investigated compounds, and used standard Molecular Operating Environment (MOE) descriptors as well as a multitude of novel hypothesis-driven molecular descriptors, like k , n_{pdN} , CSA and calculated lysosomal drug concentration (Table 5). We did not use 3D-descriptors, which depend on stereoisomers, preprocessing and energy minimization. Furthermore, we made use of size-intensive descriptors. Remarkably, none of the descriptors of the final model was a standard MOE-descriptor. We applied machine learning algorithms with a low proneness to overfitting (random forest) and performed a rigorous model validation (bootstrap). Our performance measure was well suited for dysbalanced bimodal data (Youden-index). We thus developed a simple model with high internal consistency, high external predictivity (mean bootstrapped accuracy of about 87% in the experimental set), and with a mechanistic interpretation. Finally, we introduce a new measure for comparison of structural heterogeneity between sets of compounds (div_{rel}).

Limitations: The chemoinformatic model presented here is valid for small drug-like molecules only. The model allows the qualitative prediction only. The effect of a substance on ASM activity under therapeutic conditions *in vivo* depends on the interplay between compound-, treatment- (such as dose and application route) and organism-related variables. Future studies should clarify whether or not functional inhibition of ASM occurs at therapeutic concentrations of the drugs investigated here.

Conclusions

Functional inhibitors of ASM (FIASMAs) are an important class of drugs with newly emerging broad clinical applications. In the present study we have identified 27 novel FIASMAs. Based on a large set of experimental data, we have developed a chemoinformatic model for the accurate prediction of functional inhibition of ASM. Furthermore, we describe important properties of FIASMAs, such as BBB permeability.

Materials and Methods

Set of compounds

In addition to the set of 101 compounds previously experimentally investigated with regard to functional inhibition of ASM [52], we selected 175 small organic, drug-like compounds or natural products. The selection aimed at obtaining compounds with high structural diversity, with diversity regarding strength and number of acidic and basic functional groups, and diversity regarding logP values. Basic lipophilic compounds were overrepresented in order to obtain a sufficient number of FIASMAs and in order to avoid a greatly unbalanced class distribution for classification tasks. Of the total set of 276 compounds (Table S1) with a mean molecular weight of 359.9 (88.2–847.0), 23 were acids with a most acidic pKa-value as estimated by ACD10 [86] below 10 and no relevant basic group ("acid") and 155 were weak bases with a most basic

Table 5. List of programmed and calculated descriptors that were used in addition to the standard MOE-descriptors.

Name of the descriptor	Description
AA	Length of the amphiphilic axis [95]
CSA	Cross-sectional area [95]
NOOM	Number of atoms outside the amphiphilic axis [95]
Li	Longest distance from an ionized atom to another atom [95]
Mpc	Longest distance from the atom with the highest partial charge [95]
n_qN	Number of quaternary nitrogen atoms
n_COOH	Number of carboxylic acid functions [133]
n_OpN	Sum of nitrogen and oxygen atoms [134]
n_hal	Number of halogen atoms (based on: Norinder and Haerberlein [134])
n_XpC	Sum of halogen and carbon atoms (based on: Norinder and Haerberlein [134])
n_ion	Number of ionized atoms (based on: Lanevskij et al. [56])
n_pI	Number of positive ionizable groups (based on: Lanevskij et al. [56])
n_pdN	Number of protonized delocalized nitrogen atoms in the N-C=N motif
n_pH	Number of polar hydrogen atoms [135]
n_pol	Number of polar atoms [135]
n_amines	Number of amines
n_pN	number of protonated nitrogen atoms at pH 7
I3	+1 for amines, -1 for acids, otherwise 0 [136]
QMAXneg	Highest negative partial charge [133]
QMAXpos	Highest positive partial charge [133]
QMEANN	Average partial charge in nitrogen atoms
QSUMH	Sum of all partial charges on hydrogen atoms
QSUMO	Sum of all partial charges on oxygen atoms [133]
QMINN	Lowest partial charge on nitrogen atoms
QSUMN	Sum of all partial charges on nitrogen atoms
Qamines	Average partial charge on amines
CLys	Calculated lysosomal concentration [49]
LA	Lipoaffinity [137]
logPACD10_minus_O_N	LogP - number of oxygen and nitrogen atoms [134]
logPACD10_logWeight	logPACD10 - 1/2*logWeight [56,57]
pKa1_plus_pKa2ACD10	pKa1ACD10+pKa2ACD10
pKa1_plus_pKa2ACD10mod	if pKa2ACD10>0: pKa1ACD10 + pKa2ACD10, else: pKa1ACD10
si_Weight-Descriptors	Size-intensive descriptors [96] using molecular weight as divisor

doi:10.1371/journal.pone.0023852.t005

pKa-value ≥ 3 and neither another relevant basic nor any relevant acidic group (“monobase”). Further 22 compounds possessed both a basic nitrogen atom with a pKa-value ≥ 3 and an acidic group with a pKa-value below 10 (“zwitter”). Additional 45 compounds contained two basic nitrogen atoms both with pKa-values ≥ 3 and no relevant acidic group (“bibase”). The remaining 31 compounds either had no ionisable functional group at all (n = 9) or had pKa-values outside the biologically relevant range (n = 22).

Structure entry

Molecular structures were obtained from the PubChem-Project page [87,88] (Table S1).

Chemicals

Aclacinomycin-A **133**, acrivastine **134**, amorolfine **139**, clonidine **173**, lynestrenol **228**, montelukast **239** and rolipram **271** were purchased from Biotrend Chemikalien (Köln,

Germany); phenylmethylsulfonyl fluoride **253** and S-methylsothiourrea **274** from Calbiochem (Merck, Darmstadt, Germany); allylestrenol **135**, atovaquone **142**, barnidipine **146**, butenafine **155**, cepharanthine **161**, chlorquinaldol **166**, clemastine **170**, dienestrol **187**, dutasteride **195**, nelfinavir **243**, solasodine **278** and vinblastine **299** from Chemos (Regenstauf, Germany) and dimebon **189** from Aurora Feinchemie (Graz, Austria). Apomorphin **140**, doxorubicin **193**, phenserine **251**, pranlukast **257**, raloxifene **266** and zolantidine (SKB41) **306** were obtained from Tocris (Bristol, UK) and aprindine **141**, biperidene **149**, buclicine **152**, buspiron **154**, diosmin **190**, emetine **196**, encainide **197**, fosinopril **211**, hydroxyzin **219**, ropinirole **272**, thiocarlide **287**, tiagabine **288** and zafirlukast **305** from VWR (Darmstadt, Germany). Quetiapine **264** was a gift of AstraZeneca (Wedel, Germany). All other substances investigated experimentally were obtained from Sigma-Aldrich (Munich, Germany). All compounds were used in the highest purity available.

Cell culture

Human brain neuroglioma H4-cells were purchased from Promochem (Wesel, Germany). H4-cells were cultured as described previously [52]. Only cells tested negative for mycoplasma infection were used in the experiments.

Kinetics of lysosomal accumulation

Usually, 30 min of incubation of H4-cells with the test drug was sufficient to induce functional inhibition of ASM. Due to slow accumulation kinetics some compounds required a longer incubation time. However, prolonged incubation with some compounds (astemizole **43**, mibefradil **74**, penfluridol **79**, fluoxetine **104**, sertindole **249**, thioridazine **32**) resulted in cell death. We therefore aimed at a minimal but still sufficient incubation time for all compounds, which was estimated using a previously developed numerical single cell model [49]: Accumulation of molecules in the cell by diffusion from the external solution into the cytosol, lysosome and mitochondria was calculated with the Fick-Nernst-Planck-equation. The cell model considers the diffusion of neutral and ionic molecules across biological membranes, dissociation into mono- or bivalent ions, adsorption to lipids, and electrical attraction or repulsion. We used the parameters of the standard model [49] as well as the $\log P$ -, most basic and most acidic pK_a -values as calculated by ACD10 [86] (Table S1). Four different models (“monoacid”, “monobase”, “bibase” and “zwitter”) implemented in Excel sheets were used for kinetic calculations (model version: July 2009). There was no amphoteric compound in our dataset. In the absence of pK_a -values in the relevant regions, the monoacid model was used with a pK_a -value of 15.

Experimental determination of ASM activity

The activity of ASM was determined in whole cell lysates, as previously described [89]. We aimed to develop a qualitative (binary) SPAR model. Therefore, we did not determine IC50 values, but we determined whether or not a compound acts as functional inhibitor of ASM. Thus, we used a single high concentration of a compound and a sufficient incubation time, which depends on the pharmacokinetic properties of the compound. After the substance was added to the growth medium at a final concentration of 10 μ M, cells were kept at 37°C in a humidified atmosphere at 8.5% CO₂ for 30 minutes (DMEM: pH 7.5). Compounds with predicted slow lysosomal accumulation kinetics [49] were also investigated at longer incubation times (Table S1). Results are given as residual ASM activity (%) normalized to control cells treated with the solvent alone and represent mean values of three independent experiments, each with a standard deviation of approx. 16%. Because of the bimodal distribution of functional inhibition of ASM (see below), a residual ASM activity $\leq 50.0\%$ in H4-cells was rated as positive.

Statistical analysis

Deviation from normal distribution (two-sided Kolmogoroff-Smirnov) and chi-square statistics were computed using PASW (Version 18, Chicago, Illinois). One-sided Fisher’s exact probability test with Benjamini-Hochberg [90] correction for multiple testing was computed using R software (version version 2.7.0) [91].

Computation of molecular descriptors

Molecular descriptors were calculated by the ACD/LogD Suite, version 10 [86] (the two most basic pK_a -values, the most acidic pK_a -value, $\log P$ -value), by visual inspection of the molecules [number of heavy atoms at the most basic nitrogen atom (k [52])

and by MOE 2009.10 [92]. The lysosomal concentration of each drug was calculated by a previously developed numerical single cell model [49] (see above) and was also used as a molecular descriptor (CLys). It has previously been suggested that the lowest cross-sectional area of a molecule perpendicular to the amphiphilic axis determines the insertion of a molecule into a biomembrane and thereby its passive diffusion across the BBB [93,94]. The lowest cross-sectional area (CSA, Table 5) of the molecules perpendicular to the amphiphilic axis in the membrane bound conformation and related molecular descriptors were calculated as previously described [95]. A simple division of molecular descriptors by chemical sample size creates size-intensive descriptors which were shown to result in more compact and more stable models [96]. We used molecular weight (MW) to calculate a size-intensive form of every molecular descriptor. Furthermore, we used an MW-based correction of $\log P$ -values ($\log P - \frac{1}{2} \log \text{Weight}$ [56,57]). Further information on these descriptors is available in Table 5 and in the literature [59,97].

Data pre-processing

Data pre-processing was performed using RapidMiner 5.1 [98]. Features with very low variance were eliminated. Missing values for the most basic pK_a -values were substituted by 0, missing most acidic pK_a -values were substituted by 15, missing values for k were substituted by 12. Otherwise, we used only molecular descriptors that were available for all compounds and thereby obtained a total of 708 molecular descriptors. The presence of irrelevant and redundant attributes may reduce the performance of learners such as decision tree and random forest [99]. Therefore, before applying random forest learners we reduced the dimensionality of the data by applying feature selection methods. We used both a hypothesis-driven and a hypothesis-free feature selection approach [100,101] to select descriptors with potential relevance. For the hypothesis-free selection, attributes were chosen by at least one of the following methods: wrapper [102], relief [103,104], correlation based weighting, information gain weighting, standard deviation based weighting, support vector machine based weighting and rule based weighting. We thus ended up with about 100 molecular descriptors used for random forest learners.

Model construction

Models were generated using machine learning algorithms [105,106] provided by RapidMiner 5.1 [98]. The whole experimental set was used, since examples are too precious to waste during model generation [107]. A modified beam-search [108] served to identify high-performing single attributes or attribute combinations. Models were validated by bootstrapping (n = 200). Because of the unbalanced class distribution, the Youden-Index [109–111] (sensitivity + specificity – 1) was chosen as primary performance measure evaluating models based on two-class learners. We used a random forest learner [112] for binary classification. In contrast to a simple decision tree learner, random forest learners are more resistant against overfitting and result in more stable models, meaning that small changes in the training set do not lead to completely different models [113,114], and lead to better predictivity on unknown compounds. The parameters used were: ntree = 51 (number of trees to build), nodesize = 1 (size of the terminal node of the trees in a random forest), mtry = $\log(m)+1$ (number of attributes randomly selected at each node, where m = number of attributes available), allowed maximal depth of the trees = 8.

Whenever a structure activity relations (SAR) model is built, there is a probability that the best model is chance correlation. We

used the response permutation test, also known as Y-scrambling [59–61,115] to detect random effects.

Relative structural diversity of the set of compounds used

In order to estimate the structural diversity of our investigated sets of compounds, we performed a hierarchical clustering based on Tanimoto coefficients [67] for fingerprints based on tagged graph triangles (TGT) [116,117]. We calculated the number of clusters at 0.85 similarity measured by Tanimoto coefficients and divided it by the total number of compounds in the test set. We term this measure “relative structural diversity” (div_{rel}).

$$div_{rel} = \frac{n_{cluster}}{n_{total}}$$

Higher values for div_{rel} indicate higher structural diversity. The values for div_{rel} can vary from just above zero (when there is only one cluster) to 1 (when each compound defines a separate cluster). For our analysis, we have used the structural TGT keys [116,117] consisting of 2D pharmacophore features with atom types and distances.

Violation of Lipinski's Rule-of-Five

Lipinski's Rule-of-Five [65] identifies compounds with properties that would likely make them an orally active drug in humans. The set of four rules describes molecular properties important for a drug's pharmacokinetic properties in the human organism, including its absorption, distribution, metabolism, excretion and toxicity (ADME/Tox). Violation of Lipinski's Rule-of-Five was calculated by ACD10 logD Suite. Violation was assumed when there was a contradiction to any of the four rules.

Data on passive diffusion across the blood-brain barrier

The most common value describing permeability across the blood-brain barrier (BBB) is the logBB. It is defined as the logarithmic ratio between the concentration of a compound in brain and blood. LogBB values below zero indicate poor penetration of the BBB. LogBB values were compiled from a number of published papers [58,118–128].

Distribution of FIASMAs across the therapeutic and structural classes of the ATC system

The five-level ATC drug classification system [69,129,130] was developed in the early 1970s and provides a comprehensive and logical classification system for categorizing pharmaceutical ingredients approved for medical use in humans. While the first level indicates the main anatomical target of the compound, the second level codes for the pharmacologically-relevant therapeutic main group. The third level indicates the pharmacological subgroup and the fourth the chemical subgroup. The fifth level represents the chemical substance, namely the actual drug entity. On the first level, the code comprises 14 anatomical regions ranging from A (Alimentary tract and metabolism) to V (Various). On the second level, the code consists of 86 pharmacologically-relevant therapeutic groups. Molecular structures of the drugs in

their corresponding free base/acid forms were obtained from the SuperDrug database [131]. Export was performed in May 2007, based on the 2005 version of the ATC system. Since we analyzed molecular descriptors of defined molecules, our approach excluded drugs which are entire plants, extracts, drug mixtures, colloids, biopolymers, resins, large peptides and inorganic substances like metals and simple salts. Furthermore, we excluded compounds with a quaternary nitrogen atom, as they do not cross biological membranes via passive diffusion [56]. All compounds were analyzed by their appearance in the ATC system, i.e. substances with multiple effects and different therapeutic indications or different enantiomeric forms were found more than once within the system. In order to determine the distribution of drugs across the ATC system, we used the second level of the 2005 version. Uneven distribution of FIASMAs was tested by a contingency table and one-sided Fisher test. Within this contingency table, the multiple test correction (Benjamini-Hochberg [90]) identified therapeutic groups with a significantly enriched fraction of FIASMAs [132].

Distribution of FIASMAs across natural products

Molecular structures of “Pure Natural Products” were downloaded from MicroSourceDiscovery [66] and analysed using the random forest model based on the whole experimental set. This set of “Pure Natural Products” consisted of 800 alkaloids, flavonoids, sterols/triterpenes, diterpenes/sesquiterpenes, benophenones/chalcones/stilbenes, limonoids/quassinoids and chomones/coumarines, benzofurans/benzopyrans, rotenoids/xanthones, carbohydrates and benzotropolones/depsides/depsidones. Compounds with a quaternary nitrogen atom and duplicates were again excluded from this analysis.

Supporting Information

Table S1 Compounds investigated in this study. (DOC)

Acknowledgments

We thank Andrea Leicht, Michaela Schäfer and Alice Konrad for excellent technical assistance, Torsten Kuwert (Department for Nuclear Medicine, University Hospital Erlangen) for support with the use of the radio-nucleotide facility and Elisabeth Naschberger (Division of Molecular and Experimental Surgery, University Hospital Erlangen) for support with quantifying radioactivity. We would like to thank Robert Preissner (Berlin Center of Genome Based Bioinformatics, Charité) for providing molecular structures of compounds contained in the ATC-system by a special export from the SuperDrug databank. Quetiapine **264** was a gift of AstraZeneca (Wedel, Germany). MicroDiscovery (Berlin) calculated the contingency table statistics. Rapid-I GmbH (Dortmund, Germany) implemented new operators and parameters into the RapidMiner software, rendering it suitable for developing SAR models.

Author Contributions

Conceived and designed the experiments: JK EG MM PT. Performed the experiments: PT AF SP. Analyzed the data: JK MM ST. Wrote the paper: JK MM PT. Provided intellectual input: ST MR CM LT TWG GMS KRL EG.

References

- Jin S, Yi F, Zhang F, Poklis JL, Li PL (2008) Lysosomal targeting and trafficking of acid sphingomyelinase to lipid raft platforms in coronary endothelial cells. *Arterioscler Thromb Vasc Biol* 28: 2056–2062.
- Hannun YA, Luberto C (2000) Ceramide in the eukaryotic stress response. *Trends Cell Biol* 10: 73–80.
- Castillo SS, Levy M, Thaikootathil JV, Goldkorn T (2007) Reactive nitrogen and oxygen species activate different sphingomyelinases to induce apoptosis in airway epithelial cells. *Exp Cell Res* 313: 2680–2686.
- Grassmé H, Jekle A, Riehle A, Schwarz H, Berger J, et al. (2001) CD95 signaling via ceramide-rich membrane rafts. *J Biol Chem* 276: 20589–20596.

5. Grassmé H, Jendrossek V, Riehle A, von Kürthy G, Berger J, et al. (2003) Host defense against *Pseudomonas aeruginosa* requires ceramide-rich membrane rafts. *Nat Med* 9: 322–330.
6. Gulbins E, Bissonnette R, Mahboubi A, Martin S, Nishioka W, et al. (1995) FAS-induced apoptosis is mediated via a ceramide-initiated RAS signaling pathway. *Immunity* 2: 341–351.
7. Chung HS, Park SR, Choi EK, Park HJ, Griffin RJ, et al. (2003) Role of sphingomyelin-MAPKs pathway in heat-induced apoptosis. *Exp Mol Med* 35: 181–188.
8. Rebillard A, Rioux-Leclercq N, Muller C, Bellaud P, Jouan F, et al. (2008) Acid sphingomyelinase deficiency protects from cisplatin-induced gastrointestinal damage. *Oncogene* 27: 6590–6595.
9. Santana P, Peña LA, Haimovitz-Friedman A, Martin S, Green D, et al. (1996) Acid sphingomyelinase-deficient human lymphoblasts and mice are defective in radiation-induced apoptosis. *Cell* 86: 189–199.
10. Kirschnek S, Paris F, Weller M, Grassmé H, Ferlinz K, et al. (2000) CD95-mediated apoptosis *in vivo* involves acid sphingomyelinase. *J Biol Chem* 275: 27316–27323.
11. Jenkins RW, Canals D, Hannun YA (2009) Roles and regulation of secretory and lysosomal acid sphingomyelinase. *Cell Signal* 21: 836–846.
12. Schwarz A, Futerman AH (1997) Distinct roles for ceramide and glucosylceramide at different stages of neuronal growth. *J Neurosci* 17: 2929–2938.
13. Futerman AH, Hannun YA (2004) The complex life of simple sphingolipids. *EMBO Rep* 5: 777–782.
14. Hobson JP, Rosenfeldt HM, Barak LS, Olivera A, Poulton S, et al. (2001) Role of the sphingosine-1-phosphate receptor EDG-1 in PDGF-induced cell motility. *Science* 291: 1800–1803.
15. Spiegel S, Milstien S (2002) Sphingosine 1-phosphate, a key cell signaling molecule. *J Biol Chem* 277: 25851–25854.
16. Toman RE, Payne SG, Watterson KR, Maceyka M, Lee NH, et al. (2004) Differential transactivation of sphingosine-1-phosphate receptors modulates NGF-induced neurite extension. *J Cell Biol* 166: 381–392.
17. Spiegel S, Merrill AH, Jr. (1996) Sphingolipid metabolism and cell growth regulation. *FASEB J* 10: 1388–1397.
18. Cuvillier O, Pirianov G, Kleuser B, Vanek PG, Coso OA, et al. (1996) Suppression of ceramide-mediated programmed cell death by sphingosine-1-phosphate. *Nature* 381: 800–803.
19. Spiegel S, Cuvillier O, Edsall LC, Kohama T, Menzeleev R, et al. (1998) Sphingosine-1-phosphate in cell growth and cell death. *Ann NY Acad Sci* 845: 11–18.
20. Brady RO, Kanfer JN, Mock MB, Fredrickson DS (1966) The metabolism of sphingomyelin. II. Evidence of an enzymatic deficiency in Niemann-Pick disease. *Proc Natl Acad Sci U S A* 55: 366–369.
21. Schuchman EH, Miranda SRP (1997) Niemann-Pick disease: Mutation update, genotype/phenotype correlations, and prospects for genetic testing. *Genet Test* 1: 13–19.
22. Smith EL, Schuchman EH (2008) The unexpected role of acid sphingomyelinase in cell death and the pathophysiology of common diseases. *FASEB J* 22: 3419–3431.
23. Kornhuber J, Medlin A, Bleich S, Jendrossek V, Henkel AW, et al. (2005) High activity of acid sphingomyelinase in major depression. *J Neural Transm* 112: 1583–1590.
24. Schwarz E, Prabakaran S, Whitfield P, Major H, Lewke FM, et al. (2008) High throughput lipidomic profiling of schizophrenia and bipolar disorder brain tissue reveals alterations of free fatty acids, phosphatidylcholines, and ceramides. *J Proteome Res* 7: 4266–4277.
25. Kornhuber J, Reichel M, Tripal P, Groemer TW, Henkel AW, et al. (2009) The role of ceramide in major depressive disorder. *Eur Arch Psychiatry Clin Neurosci* 259: S199–S204.
26. Ndengele MN, Cuzzocrea S, Masini E, Vinci MC, Esposito E, et al. (2009) Spinal ceramide modulates the development of morphine antinociceptive tolerance via peroxynitrite-mediated nitroxidative stress and neuroimmune activation. *J Pharmacol Exp Ther* 329: 64–75.
27. Malaplate-Armand C, Florent-Béchar S, Youssef I, Koziol V, Sponne I, et al. (2006) Soluble oligomers of amyloid- β peptide induce neuronal apoptosis by activating a cPLA₂-dependent sphingomyelinase-ceramide pathway. *Neurobiol Dis* 23: 178–189.
28. He X, Huang Y, Li B, Gong C-X, Schuchman EH (2010) Deregulation of sphingolipid metabolism in Alzheimer's disease. *Neurobiol Aging* 31: 398–408.
29. Han X, Holtzman M, McKeel DW, Jr., Kelley J, Morris JC (2002) Substantial sulfate deficiency and ceramide elevation in very early Alzheimer's disease: potential role in disease pathogenesis. *J Neurochem* 82: 809–818.
30. Cuzzocrea S, Deigner H-P, Genovese T, Mazzon E, Esposito E, et al. (2009) Inhibition of ceramide biosynthesis ameliorates pathological consequences of spinal cord injury. *Shock* 31: 634–644.
31. Mikati MA, Zeinich M, Habib RA, El HJ, Rahmeh A, et al. (2008) Changes in sphingomyelinases, ceramide, Bax, Bcl₂, and caspase-3 during and after experimental status epilepticus. *Epilepsy Res* 81: 161–166.
32. Kolesnick R (2002) The therapeutic potential of modulating the ceramide/sphingomyelin pathway. *J Clin Invest* 110: 3–8.
33. Gulbins E, Li PL (2006) Physiological and pathophysiological aspects of ceramide. *Am J Physiol Regul Integr Comp Physiol* 290: R11–R26.
34. Thevissen K, François IEJA, Winderickx J, Pannecouque C, Cammue BPA (2006) Ceramide involvement in apoptosis and apoptotic diseases. *Mini Rev Med Chem* 6: 699–709.
35. Deigner HP, Haberkorn U, Kinscherf R (2000) Apoptosis modulators in the therapy of neurodegenerative diseases. *Expert Opin Investig Drugs* 9: 747–764.
36. Pandey S, Murphy RF, Agrawal DK (2007) Recent advances in the immunobiology of ceramide. *Exp Mol Pathol* 82: 298–309.
37. Raff MC, Barres BA, Burne JF, Coles HS, Ishizaki Y, et al. (1993) Programmed cell death and the control of cell survival: lessons from the nervous system. *Science* 262: 659–700.
38. Kornhuber J, Retz W, Riederer P (1995) Slow accumulation of psychotropic substances in the human brain. Relationship to therapeutic latency of neuroleptic and antidepressant drugs? *J Neural Transm Suppl* 46: 311–319.
39. Kornhuber J, Tripal P, Reichel M, Mühle C, Rhein C, et al. (2010) Functional inhibitors of acid sphingomyelinase (FIASMAs): a novel pharmacological group of drugs with broad clinical applications. *Cell Physiol Biochem* 26: 9–20.
40. Testai FD, Landek MA, Goswami R, Ahmed M, Dawson G (2004) Acid sphingomyelinase and inhibition by phosphate ion: role of inhibition by phosphatidyl-*myo*-inositol 3,4,5-triphosphate in oligodendrocyte cell signaling. *J Neurochem* 89: 636–644.
41. Kölzer M, Arenz C, Ferlinz K, Werth N, Schulze H, et al. (2003) Phosphatidylinositol-3,5-bisphosphate is a potent and selective inhibitor of acid sphingomyelinase. *Biol Chem* 384: 1293–1298.
42. Sakata A, Ochiai T, Shimeno H, Hikishima S, Yokomatsu T, et al. (2007) Acid sphingomyelinase inhibition suppresses lipopolysaccharide-mediated release of inflammatory cytokines from macrophages and protects against disease pathology in dextran sulphate sodium-induced colitis in mice. *Immunology* 122: 54–64.
43. Darroch PI, Dagan A, Granot T, He X, Gatt S, et al. (2005) A lipid analogue that inhibits sphingomyelin hydrolysis and synthesis, increases ceramide, and leads to cell death. *J Lipid Res* 46: 2315–2324.
44. Mintzer RJ, Appell KC, Cole A, Johns A, Pagila R, et al. (2005) A novel high-throughput screening format to identify inhibitors of secreted acid sphingomyelinase. *J Biomol Screen* 10: 225–234.
45. Albouz S, Hauw JJ, Berwald-Netter Y, Boutry JM, Bourdon R, et al. (1981) Tricyclic antidepressants induce sphingomyelinase deficiency in fibroblast and neuroblastoma cell cultures. *Biomedicine* 35: 218–220.
46. Yoshida Y, Arimoto K, Sato M, Sakuragawa N, Arima M, et al. (1985) Reduction of acid sphingomyelinase activity in human fibroblasts induced by AY-9944 and other cationic amphiphilic drugs. *J Biochem (Tokyo)* 98: 1669–1679.
47. Sakuragawa N, Sakuragawa M, Kuwabara T, Pentchev PG, Barranger JA, et al. (1977) Niemann-Pick disease experimental model: sphingomyelinase reduction induced by AY-9944. *Science* 196: 317–319.
48. de Duve C, de Barse T, Poole B, Trouet A, Tulken P, et al. (1974) Lysosomotropic agents. *Biochem Pharmacol* 23: 2495–2531.
49. Trapp S, Rosania GR, Horobin RW, Kornhuber J (2008) Quantitative modeling of selective lysosomal targeting for drug design. *Eur Biophys J* 37: 1317–1328.
50. Kölzer M, Werth N, Sandhoff K (2004) Interactions of acid sphingomyelinase and lipid bilayers in the presence of the tricyclic antidepressant desipramine. *FEBS Lett* 559: 96–98.
51. Hurwitz R, Ferlinz K, Sandhoff K (1994) The tricyclic antidepressants desipramine causes proteolytic degradation of lysosomal sphingomyelinase in human fibroblasts. *Biol Chem Hoppe Seyler* 375: 447–450.
52. Kornhuber J, Tripal P, Reichel M, Terfloth L, Bleich S, et al. (2008) Identification of new functional inhibitors of acid sphingomyelinase using a structure-property-activity relation model. *J Med Chem* 51: 219–237.
53. Altman DG, Royston P (2006) The cost of dichotomising continuous variables. *BMJ* 332: 1080.
54. Streiner DL (2002) Breaking up is hard to do: The heartbreak of dichotomizing continuous data. *Can J Psychiatry* 47: 262–266.
55. Ragland DR (1992) Dichotomizing continuous outcome variables: Dependence of the magnitude of association and statistical power on the cutpoint. *Epidemiology* 3: 434–440.
56. Lanevskij K, Japertas P, Didziapetris R, Petrauskas A (2009) Ionization-specific prediction of blood-brain permeability. *J Pharm Sci* 98: 122–134.
57. Levin VA (1980) Relationship of octanol/water partition coefficient and molecular weight to rat brain capillary permeability. *J Med Chem* 23: 682–684.
58. Zhang L, Zhu H, Oprea TI, Golbraikh A, Tropsha A (2008) QSAR modeling of the blood-brain barrier permeability for diverse organic compounds. *Pharm Res* 25: 1902–1914.
59. Todeschini R, Consonni V (2000) Handbook of Molecular Descriptors. Weinheim, Germany: Wiley-VCH. 667 p.
60. Tropsha A, Gramatica P, Gombar VK (2003) The importance of being earnest: Validation is the absolute essential for successful application and interpretation of QSPR models. *QSAR Comb Sci* 22: 69–77.
61. von der Voet H (1994) Comparing the predictive accuracy of models using a simple randomization test. *Chemom Intell Lab Syst* 25: 313–323.
62. [Anonymous] (2007) Guidance document on the validation of (quantitative) structure-activity relationship [(Q)SAR] models. OECD: Organisation for economic co-operation and development. IOMC: Inter-organization programme for the sound management of chemicals No. 69: 1–154.
63. Bradbury MW (1993) The blood-brain barrier. *Exp Physiol* 78: 453–472.

64. Cecchelli R, Berezowski V, Lundquist S, Culot M, Renftel M, et al. (2007) Modelling of the blood-brain barrier in drug discovery and development. *Nat Rev Drug Discov* 6: 650–661.
65. Lipinski CA, Lombardo F, Dominy BW, Feeney PJ (1997) Experimental and computational approaches to estimate solubility and permeability in drug discovery and developmental settings. *Adv Drug Deliv Rev* 23: 3–25.
66. Micro Source Discovery Pure Natural Products. Available: <http://www.msdiscovery.com/natprod.html>. Accessed: 2011 Aug 12.
67. Willett P (2006) Similarity-based virtual screening using 2D fingerprints. *Drug Discov Today* 11: 1046–1053.
68. Akella LB, Decaprio D (2010) Cheminformatics approaches to analyze diversity in compound screening libraries. *Curr Opin Chem Biol* 14: 325–330.
69. The WHO Collaborating Centre for Drug Statistics Methodology, Norwegian Institute of Public Health The ATC/DDD System. Available: <http://www.whocc.no/atcddd/>. Accessed: 2011 Aug 12.
70. [Anonymous] (2007) Approved Drug Products with Therapeutic Equivalence Evaluations U.S. Department of Health and Human Services. Food and Drug Administration. Center for Drug Evaluation and Research. Office of Pharmaceutical Science. Office of Generic Drugs.
71. Yu ZF, Nikolova-Karakashian M, Zhou D, Cheng G, Schuchman EH, et al. (2000) Pivotal role for acidic sphingomyelinase in cerebral ischemia-induced ceramide and cytokine production, and neuronal apoptosis. *J Mol Neurosci* 15: 85–97.
72. Altura BM, Gebrewold A, Zheng T, Altura BT (2002) Sphingomyelinase and ceramide analogs induce vasoconstriction and leukocyte-endothelial interactions in cerebral venules in the intact rat brain: Insight into mechanisms and possible relation to brain injury and stroke. *Brain Res Bull* 58: 271–278.
73. Pascual M, Valles SL, Renau-Piqueras J, Guerri C (2003) Ceramide pathways modulate ethanol-induced cell death in astrocytes. *J Neurochem* 87: 1535–1545.
74. Paris F, Fuks Z, Kang A, Capodiceci P, Juan G, et al. (2001) Endothelial apoptosis as the primary lesion initiating intestinal radiation damage in mice. *Science* 293: 293–297.
75. Van Veldhoven PP, Matthews TJ, Bolognesi DP, Bell RM (1992) Changes in bioactive lipids, alkylacylglycerol and ceramide, occur in HIV-infected cells. *Biochem Biophys Res Commun* 187: 209–216.
76. De Simone C, Cifone GM, Roncaioli P, Moretti S, Famularo G, et al. (1996) Ceramide, AIDS and long-term survivors. *Immunol Today* 17: 48.
77. Pantaleo G, Menzo S, Vaccarezza M, Graziosi C, Cohen OJ, et al. (1995) Studies in subjects with long-term nonprogressive human immunodeficiency virus infection. *N Engl J Med* 332: 209–216.
78. Haimovitz-Friedman A, Cordon-Cardo C, Bayoumy S, Garzotto M, McLoughlin M, et al. (1997) Lipopolysaccharide induces disseminated endothelial apoptosis requiring ceramide generation. *J Exp Med* 186: 1831–1841.
79. Teichgräber V, Ulrich M, Endlich N, Riethmüller J, Wilker B, et al. (2008) Ceramide accumulation mediates inflammation, cell death and infection susceptibility in cystic fibrosis. *Nat Med* 14: 382–391.
80. Becker KA, Riethmüller J, Lüth A, Döring G, Kleuser B, et al. (2010) Acid sphingomyelinase inhibitors normalize pulmonary ceramide and inflammation in cystic fibrosis. *Am J Respir Cell Mol Biol* 42: 716–724.
81. Riethmüller J, Anthonyam J, Serra E, Schwab M, Döring G, et al. (2009) Therapeutic efficacy and safety of amitriptyline in patients with cystic fibrosis. *Cell Physiol Biochem* 24: 65–72.
82. Göggel R, Winoto-Morbach S, Vielhaber G, Imai Y, Lindner K, et al. (2004) PAF-mediated pulmonary edema: a new role for acid sphingomyelinase and ceramide. *Nat Med* 10: 155–160.
83. Dawson G, Qin J (2011) Gilenya (FTY720) inhibits acid sphingomyelinase by a mechanism similar to tricyclic antidepressants. *Biochem Biophys Res Commun* 404: 321–323. doi: 10.1016/j.bbrc.2010.11.115.
84. Elojemi S, Holman DH, Liu X, El-Zawahry A, Villani M, et al. (2006) New insights on the use of desipramine as an inhibitor for acid ceramidase. *FEBS Lett* 580: 4751–4756.
85. Canals D, Perry DM, Jenkins RW, Hannun YA (2011) Drug targeting of sphingolipid metabolism: sphingomyelinases and ceramidases. *Br J Pharmacol* 163: 694–712. doi: 10.1111/j.1476-5381.2011.01279.x.
86. Advanced Chemistry Development Inc (ACD/LogD Suite). Available: <http://www.acdlabs.com>. Accessed: 2011 Aug 12.
87. National Center for Biotechnology Information USA PubChem-Project. Available: <http://pubchem.ncbi.nlm.nih.gov>. Accessed: 2011 Aug 12.
88. Wang Y, Xiao J, Suzek TO, Zhang J, Wang J, et al. (2009) PubChem: a public information system for analyzing bioactivities of small molecules. *Nucleic Acids Res* 37: W623–W633.
89. Gulbins E, Kolesnick R (2000) Measurement of sphingomyelinase activity. *Methods Enzymol* 322: 382–388.
90. Benjamini Y, Hochberg Y (1995) Controlling the false discovery rate: a practical and powerful approach to multiple testing. *J R Statist Soc B* 57: 289–300.
91. R Development Core Team R Development Core Team. Available: <http://www.r-project.org>. Accessed: 2011 Aug 12.
92. [Anonymous] MOE. Molecular Operating Environment. Available: <http://www.chemcomp.com>. Accessed: 2011 Aug 12.
93. Gerebtzoff G, Seelig A (2006) In silico prediction of blood-brain barrier permeation using the calculated molecular cross-sectional area as main parameter. *J Chem Inf Model* 46: 2638–2650.
94. Fischer H, Gottschlich R, Seelig A (1998) Blood-brain barrier permeation: Molecular parameters governing passive diffusion. *J Membr Biol* 165: 201–211.
95. Muehlbacher M, Spitzer GM, Liedl KR, Kornhuber J (2011) Critical analysis of cross-sectional area for blood-brain barrier prediction on a large scale dataset. *J Comput-Aided Mol Des*, under review; manuscript available on request (Johannes.Kornhuber@uk-erlangen.de).
96. Purvis GD, 3rd (2008) Size-intensive descriptors. *J Comput Aided Mol Des* 22: 461–468.
97. Meloun M, Bordovská S (2007) Benchmarking and validating algorithms that estimate pK_a values of drugs based on their molecular structures. *Anal Bioanal Chem* 389: 1267–1281.
98. Mierswa I, Wurst M, Klöckner R, Scholz M, Euler T (2006) YALE: Rapid prototyping for complex data mining tasks. In: Proceedings of the 12th ACM SIGKDD International Conference on Knowledge Discovery and Data Mining (KDD-06).
99. Amaratunga D, Cabrera J, Lee Y-S (2008) Enriched random forests. *Bioinformatics* 24: 2010–2014.
100. Saacs Y, Inza I, Larranaga P (2007) A review of feature selection techniques in bioinformatics. *Bioinformatics* 23: 2507–2517.
101. Guyon I, Elisseeff A (2003) An introduction of variable and feature selection. *J Machine Learning Res* 3: 1157–1182.
102. Kohavi R, John GH (1997) Wrappers for feature subset selection. *Artificial Intelligence* 97: 273–324.
103. Kononenko I (1994) Estimating attributes: Analysis and extensions of relief. In: Proceedings of the Seventh European Conference on Machine Learning Springer Verlag, pp 171–182.
104. Kira K, Rendell L (1992) The feature selection problem: traditional methods and a new algorithm. In: Proceedings of the Tenth National Conference on Artificial Intelligence. Penlo Park: AAAI Press/The MIT Press. pp 129–134.
105. Witten IH, Frank E (2005) Data Mining. Practical Machine Learning Tools and Techniques. Amsterdam: Elsevier. 525 p.
106. Alpaydin E (2008) Maschinelles Lernen. München: Oldenbourg Wissenschaftsverlag GmbH. 440 p.
107. Roecker EB (1991) Prediction error and its estimation for subset-selected models. *Technometrics* 33: 459–468.
108. Bisiani R (1987) Beam search. In: Shapiro S, Eckroth D, eds. Encyclopedia of Artificial Intelligence. New York: Wiley & Sons. pp 56–58.
109. Youden WJ (1950) Index for rating diagnostic tests. *Cancer* 3: 32–35.
110. Fluss R, Faraggi D, Reiser B (2005) Estimation of the Youden Index and its associated cutoff point. *Biom J* 47: 458–472.
111. Bush WS, Edwards TL, Dudek SM, McKinney BA, Ritchie MD (2008) Alternative contingency table measures improve the power and detection of multifactor dimensionality reduction. *BMC Bioinformatics* 9: 238.
112. Breiman L (2001) Random Forests. *Machine Learning* 45: 5–32.
113. Zhou ZH (2009) Ensemble Learning. In: Li SZ, ed. Encyclopedia of Biometrics. Berlin: Springer. pp 270–273.
114. Svetnik V, Liaw A, Tong C, Culberson JC, Sheridan RP, et al. (2003) Random forest: A classification and regression tool for compound classification and QSAR modeling. *J Chem Inf Comput Sci* 43: 1947–1958.
115. Wold S, Eriksson L (1995) Statistical validation of QSAR results. In: van de Waterbeemd H, ed. Chemometrics Methods in Molecular Design. Weinheim: VHC. pp 309–318.
116. Ewing T, Baber JC, Feher M (2006) Novel 2D fingerprints for ligand-based virtual screening. *J Chem Inf Model* 46: 2423–2431. doi: 10.1021/ci060155b.
117. Williams C (2006) Reverse fingerprinting, similarity searching by group fusion and fingerprint bit importance. *Mol Divers* 10: 311–332. doi: 10.1007/s11030-006-9039-z.
118. Narayanan R, Gunturi SB (2005) In silico ADME modelling: Prediction models for blood-brain barrier permeation using a systematic variable selection method. *Bioorg Med Chem* 13: 3017–3028.
119. Kelder J, Grootenhuys PDJ, Bayada DM, Delbressine LPC, Ploemen JP (1999) Polar molecular surface as a dominating determinant for oral absorption and brain penetration of drugs. *Pharm Res* 16: 1514–1519.
120. Garg P, Verma J (2006) In silico prediction of blood brain barrier permeability: An artificial neural network model. *J Chem Inf Model* 46: 289–297.
121. Rose K, Hall LH, Kier LB (2002) Modeling blood-brain barrier partitioning using the electrotopological state. *J Chem Inf Comput Sci* 42: 651–666.
122. Abraham MH, Ibrahim A, Zhao Y, Acree WE, Jr. (2006) A data base for partition of volatile organic compounds and drugs from blood/plasma/serum to brain, and an LFER analysis of the data. *J Pharm Sci* 95: 2091–2100.
123. Guerra A, Pérez JA, Campillo NE (2008) Artificial neural networks in ADMET modeling: prediction of blood-brain barrier permeation. *QSAR & Combinatorial Sci* 27: 586–594.
124. Kononov DA, Coomans D, Deconinck E, Heyden YV (2007) Benchmarking of QSAR models for blood-brain barrier permeation. *J Chem Inf Model* 47: 1648–1656.
125. Zerara M, Brickmann J, Kretschmer R, Exner TE (2009) Parameterization of an empirical model for the prediction of n-octanol, alkane and cyclohexane/water as well as brain/blood partition coefficients. *J Comput Aided Mol Des* 23: 105–111.

126. Vilar S, Chakrabarti M, Costanzi S (2010) Prediction of passive blood-brain partitioning: Straightforward and effective classification models based on in silico derived physicochemical descriptors. *J Mol Graph Model* 28: 899–903. doi: 10.1016/j.jmgm.2010.03.010.
127. Mente SR, Lombardo F (2005) A recursive-partitioning model for blood-brain barrier permeation. *J Comput Aided Mol Des* 19: 465–481. doi: 10.1007/s10822-005-9001-7.
128. Platts JA, Abraham MH, Zhao YH, Hersey A, Ijaz L, et al. (2001) Correlation and prediction of a large blood-brain distribution data set - an LFER study. *Eur J Med Chem* 36: 719–730.
129. [Anonymous] (1981) [The new classification of drugs: the ATC-code now introduced]. *Ugeskr Laeger* 143: 1037–1039.
130. [Anonymous] (2004) The selection and use of essential medicines. *World Health Organ Tech Rep Ser* 920: 1–127.
131. Goede A, Dunkel M, Mester N, Frommel C, Preissner R (2005) SuperDrug: a conformational drug database. *Bioinformatics* 21: 1751–1753.
132. Cox MK, Key CH (1993) Post hoc pair-wise comparisons for the chi-square test of homogeneity of proportions. *Educational and Psychological Measurement* 53: 951–962.
133. Andres C, Hutter MC (2006) CNS permeability of drugs predicted by a decision tree. *QSAR Comb Sci* 25: 305–309.
134. Norinder U, Haerberlein M (2002) Computational approaches to the prediction of the blood-brain distribution. *Adv Drug Deliv Rev* 54: 291–313.
135. Fu X-C, Wang G-P, Shan H-L, Liang W-Q, Gao J-Q (2008) Predicting blood-brain barrier penetration from molecular weight and number of polar atoms. *Eur J Pharm Biopharm* 70: 462–466.
136. Feher M, Sourial E, Schmidt JM (2000) A simple model for the prediction of blood-brain partitioning. *Int J Pharm* 201: 239–247.
137. Liu R, Sun H, So SS (2001) Development of quantitative structure-property relationship models for early ADME evaluation in drug discovery. 2. Blood-brain barrier penetration. *J Chem Inf Comput Sci* 41: 1623–1632.